ACS OMEGA

http://pubs.acs.org/journal/acsodf

Article

Peel Adhesion Strength between Epoxy Resin and Hydrated Silica Surfaces: A Density Functional Theory Study

Yosuke Sumiya, Yuta Tsuji, and Kazunari Yoshizawa*

Cite This: *ACS Omega* 2022, 7, 17393−17400

Read Online

ACCESS | Metrics & More | Article Recommendations | Supporting Information

ABSTRACT: Adhesive strength is known to change significantly depending on the direction of the force applied. In this study, the peel and tensile adhesive forces between the hydroxylated silica (001) surface and epoxy resin are estimated based on quantum chemical calculations. Here, density functional theory (DFT) with dispersion correction is used. In the peel process, the epoxy resin is pulled off from the terminal part, while in the tensile process, the entire epoxy resin is pulled off vertically. As a result of these calculations, the maximum adhesive force in the peel process is decreased to be about 40% of that in the tensile process. The adhesion force−displacement curve for the peeling process shows two characteristic peaks corresponding to the process where the adhesive molecule horizontally oriented to the surface shifts to a vertical orientation to the surface and the process where the vertical adhesive molecule is dissociated from the surface. Force decomposition analysis is performed to further understand the peel adhesion force; the contribution of the dispersion force is found to be slightly larger than that of the DFT force. This feature is common to the tensile process as well. Each force in the peel process is about 40% smaller than the corresponding force in the tensile process.

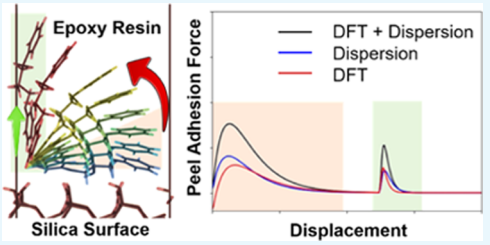

INTRODUCTION

Adhesion technology has become widespread in a variety of fields such as electronics, automobile manufacturing, construction, and medicine because of its low cost, light weight, and ease of joining dissimilar materials.[1−4] Adhesives are classified according to their main components and curing methods and selected according to the characteristics of adherends and their applications. A typical adhesive is epoxy resin, which is a highly functional polymer. It has been developed for a long time and used in many manufacturing processes, such as molding and painting.[5]

Epoxy resins are synthesized through the polymerization reaction of diglycidyl ether of bisphenol A (DGEBA) shown in Figure 1a.[6,7] It is known experimentally and theoretically that the hydroxyl groups of DGEBA interact with hydroxyl groups and coordinatively unsaturated sites on the adherend surfaces[8−16] or with water molecules adsorbed on the surfaces.[17−22] It has also been pointed out that the OH−π interaction between the benzene ring of epoxy resin and adherend surfaces also makes a non-negligible contribution to the adhesion mechanism.[23,24] Such interfacial interactions between the adhesive and adherend are considered to have significant effects on the mechanical properties of various commercial products.

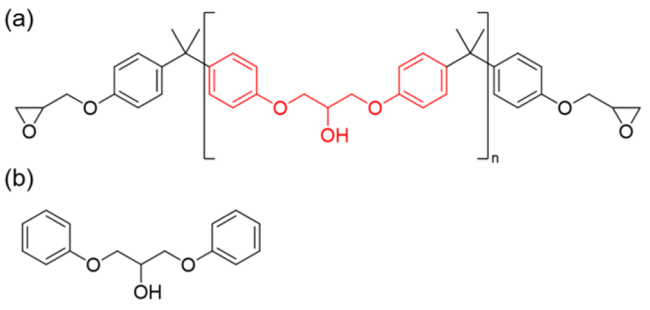

Figure 1. (a) Chemical structure of bisphenol A epoxy resin. (b) Fragmented model for the epoxy resin, which corresponds to the red part in (a).

The interfacial interaction is evaluated from the adhesive strength, which is the criterion for selecting an adhesive. The adhesion force is measured using the adhesion test defined for example by the American Society for Testing and Materials (ASTM). Figure 2 shows the examples of the adhesion test. Figure 2a−c corresponds to the tensile, peel, and shear adhesion tests, respectively. Since it is known that the adhesion force varies greatly depending on the direction of force application,[25] different adhesion tests are conducted according to the application of the product. Although theoretical studies on adhesive forces have been conducted,[8−12,14,18,21−24,26−29] many of these studies are related to tensile adhesive forces;

Received: March 15, 2022
Accepted: May 5, 2022
Published: May 14, 2022

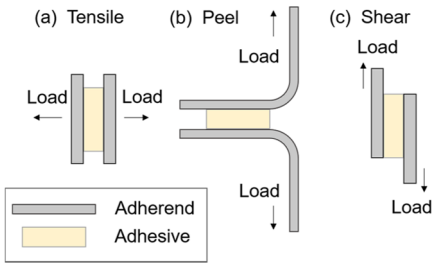

Figure 2. Typical examples of adhesion tests prescribed by ASTM. Tensile, peel, and shear adhesion strengths are measured using the methods shown in (a), (b), and (c), respectively.

theoretical methods to estimate the adhesive forces corresponding to other adhesive tests and molecular understandings for the adhesive interfaces are needed.

In this study, we focus on the peel adhesion test, calculating the adhesive strength based on density functional theory (DFT) calculations and compare its results with the tensile adhesion one. We recognize that the shear adhesion test is another important test method. The results on the shear adhesive strength will be presented in a forthcoming paper. For now, we note that it has been investigated by classical molecular dynamics (MD) calculations.[30] The peel adhesion strength was calculated for the adhesion interface between epoxy resin and the silica (001) surface, which mimics the structure of glass fiber-reinforced plastics (GFRP). Here, the silica surface was created by cleaving the bulk structure of α-cristobalite. GFRP is characterized by its combination of high specific strength, high specific stiffness, and light weight and expected to be used especially in the aircraft and aerospace fields.[31] There is a great deal of demand for insights into the changes in the interfacial interactions between epoxy resin and glass at the atomic and molecular levels as GFRP is stressed and led to failure.[32,33] Because of the complex fracture modes of GFRP, the adhesion forces in various directions between the adhesive and the silica surface have been investigated.[34,35] Therefore, in this study, we investigate the differences in these adhesion mechanisms.

MATERIALS AND METHODS

Modeling of the Periodic Interface. In this study, we used three models analyzed in our previous study[23] (see Figure 3 for the structures); see the reference for modeling details. In accordance with it, we decided to model epoxy resin using a fragment model shown in Figure 1b, which is a simplified version of the DGEBA structure (Figure 1a). Hereafter, we will refer to this model as the "epoxy molecule". These configurations were obtained from the DFT-level optimization of structures obtained from molecular dynamics (MD) simulations. Figure 3a–c shows the first, second, and third most stable structures, respectively. A stable structure has a higher existence probability and is expected to contribute primarily to the physical properties.

A periodic silica (001) surface was created by cleaving the bulk structure of α-cristobalite obtained from the Materials Studio 6.1 database.[36] The silica unit cell consists of four silicon atoms and eight oxygen atoms, with tetragonal lattice constants of $a = b = 4.93$ Å and $c = 6.80$ Å. By repeating this unit cell twice in the c-axis direction, a supercell consisting of eight atomic layers was constructed. In the present study, a vacuum layer with a thickness of about 45 Å was added on the

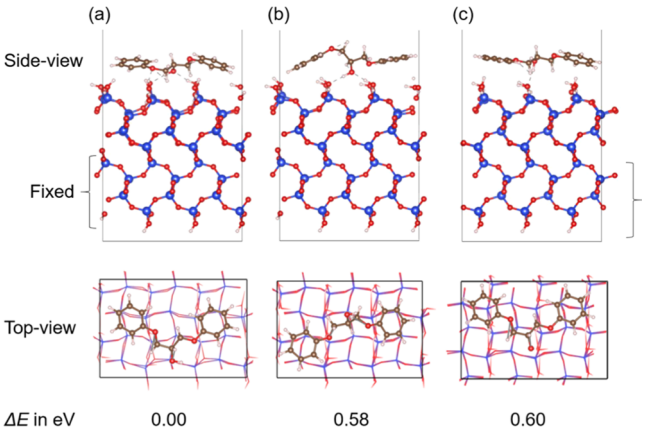

Figure 3. Three optimized structures of the epoxy molecule adsorbed on the silica (001) surface: (a) most stable, (b) second most stable, and (c) least stable structures. ΔE is the relative energy (eV) compared to the most stable structure. Red corresponds to oxygen, blue corresponds to silicon, brown corresponds to carbon, and white corresponds to hydrogen.

surface. The coordinatively unsaturated silicon atoms on the surface were passivated through the dissociative adsorption of two water molecules. For the epoxy molecule to be adsorbed on the silica surface, the slab model was extended to a 2×3 supercell so that it can accommodate the adsorbate. Here, the silica surface was optimized by fixing the atomic coordinates of the lower layer as shown in Figure 3. As such, the size of the cell was $9.86 \times 14.79 \times 60.00$ Å^3.

These models most simply describe the interaction at the interface between the epoxy resin and the surface. Here, only one side of the adherend surfaces in Figure 2 was considered. Therefore, the interaction between one adherend surface and the other adherend surface is ignored. In addition, since only one epoxy molecule is considered, the effects of epoxy resin entanglement and thickness influences are neglected. Creating a model that incorporates these effects is future work.

In the adhesive interface models created in this way, the silica surfaces are dry and in ideal condition. These models correspond to a situation where the surface is pretreated at high temperatures. A recent molecular dynamics study has reported that most interfacial water molecules are pushed out by the epoxy resins.[37] It is thus possible that a small number of water molecules at the interface might affect the adhesive strength. Investigation of this effect is the next task. In addition, the roughness of solid surfaces results from atomic vacancy, adatoms from the gas phase, steps, and kinks. These could affect adhesion, and it would be interesting to investigate these effects. However, the focus of this study is on the computational method for the peel adhesion force and its properties, and an investigation of the effects for roughness is beyond the scope of this paper. For the above-mentioned reason, the smooth surfaces were selected.

Computational Methods for the Calculation of Tensile Adhesive Strength. The adhesion force between the epoxy molecule and the silica surface was estimated from periodic boundary DFT calculations. All the DFT calculations were performed using Vienna ab initio simulation package (VASP) 5.4.4.[38−40] The Perdew−Burke−Ernzerhof form of the generalized gradient approximation (GGA-PBE) was adopted as the exchange correlation functional.[41] The D2 method by Grimme was used for dispersion correction.[42] The

https://doi.org/10.1021/acsomega.2c01544
ACS Omega 2022, 7, 17393−17400

electron−ion interaction was treated with the projector augmented wave scheme.[43,44] The cutoff of the plane wave basis set and the convergence threshold of the self-consistent field were set to 500 and 1.0×10^{-5} eV, respectively. The Brillouin zone was sampled with a spacing between k points of $2\pi \times 0.05$ Å^{-1}, and the threshold for the atomic force was set to 0.05 eV Å^{-1}.

The tensile adhesion strength was obtained by differentiating the potential energy curve, which represents the energy change during the process of the entire adhesive molecule being pulled vertically away from the surface.[8−11,17,21,22,27−29] To obtain the potential energy curve, we gradually displaced the entire epoxy molecule upward from the silica surface in increments of 0.1 Å, as shown in Figure 4a.

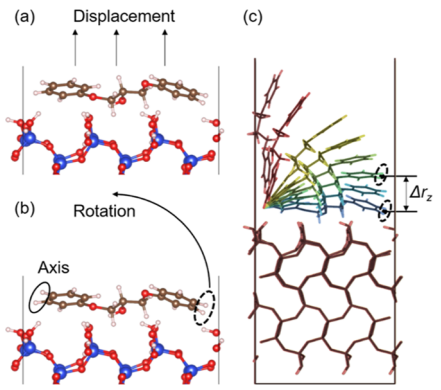

Figure 4. (a) Displacement direction of the epoxy molecule for calculating the potential energy curve that gives tensile adhesion strength. (b) Displacement direction of the epoxy molecules for calculating the potential energy curve that gives the peel adhesion strength. (c) Definition of the motion of the epoxy molecule and displacement Δr_z in the z direction during the peel process.

The structures of the epoxy molecule and silica were fixed when the displacement was applied, and a single-point calculation was performed at each point to obtain the energy. The obtained energy−displacement (ΔE−Δr_z) plot was fitted with the Morse potential of the following equation

$$E = D(1 - \exp(-a\Delta r_z))^2 \quad (1)$$

where D is the adhesion energy, a is the constant inherent to the system and related to the width of the potential well, and Δr_z is the displacement between the epoxy molecule and the silica surface from the equilibrium structure. To obtain the adhesion force−displacement ($F_z - \Delta r_z$), the fitted potential curve was differentiated with respect to Δr_z.

$$F_z = \frac{dE}{d\Delta r_z} \quad (2)$$

The tensile adhesive strength was estimated from the maximum value of F_z.

Computational Methods for the Calculation of Peel Adhesive Strength. The potential energy curve corresponding to the separation process of the adhesive (epoxy) molecule from the surface through the peel process was calculated as follows. The epoxy molecule was displaced in an arc with the hydrogen atoms surrounded by the solid line circle at the end as the axis of rotation, as denoted by "Rotation" in Figure 4b, and a single-point calculation was performed at each point of displacement to obtain the energy at each point. After the epoxy molecule became perpendicular to the surface, the upward displacement of the epoxy molecule was initiated. The displacement width of the epoxy molecule from its initial structure, Δr_z, was defined as the z-axis displacement of the center of gravity of the hydrogen atoms surrounded by the dotted line circle as shown in Figure 4c. The obtained energy−displacement (ΔE−Δr_z) plot was approximated by a polynomial equation for the Morse potential (eq 1). The specific form of this equation will be shown later. As with the tensile adhesion strength, the potential energy curve was differentiated with respect to Δr_z to obtain the peel adhesion force−displacement (F_z−Δr_z), and the maximum force value was regarded as the peel adhesion strength. In this study, the adhesion forces in the peeling direction, as shown in Figure 4b, were estimated for the three adsorption structures shown in Figure 3a−c.

RESULTS AND DISCUSSION

Peel Adhesion Force between the Epoxy Molecule and the Silica Surface. The gray dotted line in Figure 5a shows the energy change during the peel process of the epoxy molecule shown in Figure 3a from the silica (001) surface along the direction of rotation in Figure 4b. The potential energy curve is plotted in 0.1 Å increments. There are two inflection points in this energy curve. This feature of the peel process is compatible with previous studies and originates from

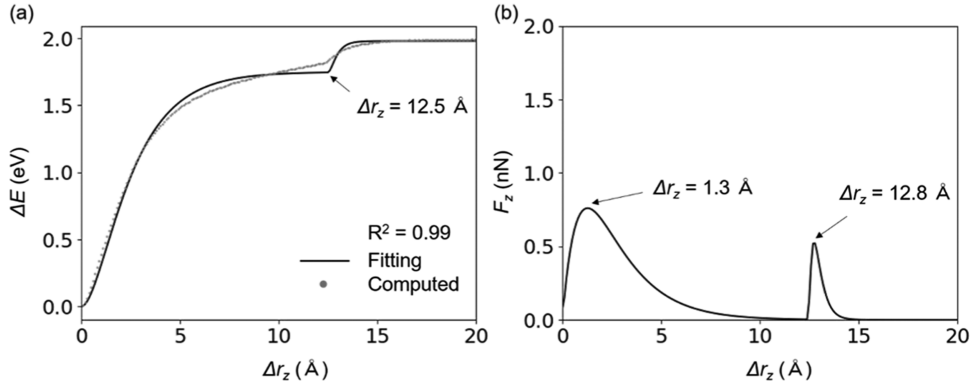

Figure 5. (a) Potential energy−displacement (ΔE−Δr_z) curve for the peel process of the epoxy molecule shown in Figure 3a. Each point in the gray dotted line corresponds to the value obtained from the calculation, and the black solid line corresponds to the curve obtained by fitting. (b) Peel adhesion force−displacement (F_z−Δr_z) curve obtained by differentiating the fitting curve in (a).

https://doi.org/10.1021/acsomega.2c01544
ACS Omega 2022, 7, 17393−17400

two events:[45−47] the first inflection point is due to the destruction of the interaction between the substructure near the displaced terminal atoms and the surface as the epoxy molecule is peeled from the surface (peel process 1) and the second inflection point is due to the destruction of the interaction between the vertical molecule and the surface (peel process 2). The Supporting Information (SI) in this paper shows the energy curves and parameters in the peel direction for all the models shown in Figure 3; they all show the same trend.

Assuming that the energy change is represented by these independent subprocesses, the energy curve can be modeled by the sum of the two functions. Therefore, in this study, the energy plot was fitted using the function expressed by the following equation

$$E = D_1(1 - \exp(-a_1\Delta r_z))^2 + H(\Delta r_z - \Delta r_p)\cdot D_2(1 - \exp(-a_2(\Delta r_z - \Delta r_p)))^2 \quad (3)$$

$$H(\Delta r_z - \Delta r_p) = \begin{cases} 1\ (\Delta r_z \geq \Delta r_p) \\ 0\ (\Delta r_z < \Delta r_p) \end{cases} \quad (4)$$

where the first and second terms in eq 3 correspond to peel processes 1 and 2, respectively, D_1 and a_1 are the parameters for the first process, D_2 and a_2 are the parameters for the second process, H is the Heaviside step function expressed in eq 4, and Δr_p corresponds to the value of Δr_z when the epoxy molecule has just become perpendicular to the surface. In the present study, Δr_p is 12.5 Å. Using H, the energy curve for the dissociation of the perpendicular epoxy molecule from the surface can be expressed by the Morse potential of the second term. The fitting curve using eq 3 is represented by the solid black line in Figure 5a, and its R^2 value is 0.99. Each parameter in eq 3 is summarized in Table 1. The gray dotted line and the black solid line are away from each other at around Δr_z = 12.5 Å, where the epoxy molecule becomes perpendicular to the surface. This suggests that the two processes are not completely independent of each other.

Table 1. Values of Parameters D_i and a_i for the Two Peeling Processes and the Maximum Values of Adhesion Forces F_i and Their Displacement Positions Δr_i

peel process i	D_i (eV)	a_i (Å^{-1})	Δr_i (Å)	F_i (nN)
i = 1	1.75	0.54	1.3	0.76
i = 2	0.23	2.94	12.8	0.52
tensile process	D (eV)	a (Å^{-1})	Δr (Å)	F (nN)
	1.90	1.19	0.6	1.80

Figure 5b shows the adhesive force−displacement (F_z−Δr_z) curve. This curve was obtained by numerically differentiating the fitting curve in Figure 5a. There are two peaks in the adhesive force curve, which correspond to the inflection points on the energy curve. The two peaks are located at Δr_1 = 1.3 Å and Δr_2 = 12.8 Å, and their adhesive forces are F_1 = 0.76 nN and F_2 = 0.52 nN, respectively. These values are also summarized in Table 1.

Tensile Adhesion Force between the Epoxy Molecule and the Silica Surface. For comparison, the tensile adhesion force was estimated for the same system. The gray dotted line in Figure 6a shows the energy change during the process of the entire epoxy molecule being pulled up vertically from the silica surface as shown in Figure 4a. The potential energy curve is plotted in 0.1 Å increments. As in many previous studies,[8−12,17,21,22,27−29] there is one inflection point in the curve. The curve was fitted using the Morse potential shown in eq 1. The R^2 value for the fitting is 1.00, and the fitting curve perfectly matches the original data. Numerical differentiation of this fitting curve yielded the adhesion force−displacement (F_z−Δr_z) curve shown in Figure 6b. The peak in the curve is located at Δr_z = 0.6 Å, and its adhesion force is F = 1.80 nN (Table 1). The SI shows the energy curves for all the models and their parameters, all of which show the same trend.

Comparing the maximum value of the peel adhesion strength, F_1, with that of the tensile adhesion strength, F, F_1 was found to be 42.2% of F. This result qualitatively reproduces the property that epoxy adhesives are fragile in the peel direction rather than the tensile direction.[25] The order of the Morse potential parameter of D is the same as that of the maximum adhesive force for each process: tensile process > peel process 1 > peel process 2. We found that the following conservation law holds for D of each process.

$$D(\text{tensile}) \approx D_1(\text{peel}) + D_2(\text{peel}) \quad (5)$$

Since D means adhesion energy, the above-mentioned equation can be interpreted as dividing the tensile adhesion energy into two, each of which corresponds to the respective peel process. This is likely to support that tensile adhesive strength is greater than peel adhesive strength. The total amount of energy change in each process is the same, but in the tensile process, the energy changes rapidly in a small displacement of a single step. On the other hand, in the peel process, the energy changes in two steps incrementally. By and large, therefore, it can be concluded that the adhesive force obtained from the energy gradient is larger in the tensile process. For both tensile and peel processes, the D values are dependent on the configuration of the epoxy molecules, and the order of D for all configurations in Figure 3a−c is the same as for the energy (Table S1).

Let us compare parameter a in the tensile process with that in peeling processes 1 and 2. The value of a for peeling process 1 is small, while that for peeling process 2 is large and that for the tensile process is in the middle of them. Since the potential width becomes smaller with larger parameter a, the peak width of the adhesive force is in the order of peel process 1 > tensile process > peel process 2. This parameter is often used to model the molecular interaction as a spring.[48] If the adhesive interface is considered as a Morse oscillator, the second-order force constant can be expressed by the harmonic approximation of the Morse potential near the minimum as follows[49]

$$k = 2a^2D \quad (6)$$

Table 2 shows the values obtained from this equation for the force constant of each adhesion process. This table indicates that the adhesive interface in the tensile process can be regarded as the hardest spring. On the other hand, the adhesive interface in peel process 1 can be regarded as the softest spring. It should also be noted that the order of the adhesive forces (F_1 and F_2) and the force constants are reversed in peel processes 1 and 2. This is due to the large difference in a. This suggests that the adhesive interface between the atoms at the rotational axis and the surface acts as a stiff spring with a small

https://doi.org/10.1021/acsomega.2c01544
ACS Omega 2022, 7, 17393−17400

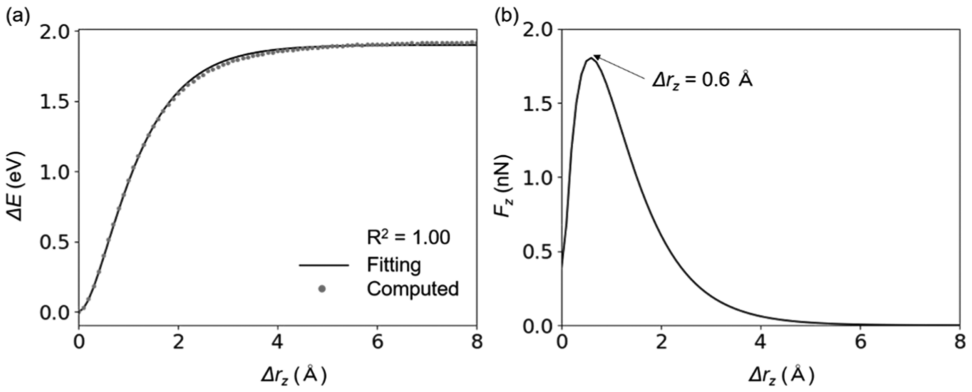

Figure 6. (a) Potential energy−displacement ($\Delta E-\Delta r_z$) curve for the tensile process of the epoxy molecule shown in Figure 3a. Each point in the gray dotted line corresponds to the value obtained from the calculation, and the black solid line corresponds to the curve obtained by fitting. (b) Tensile adhesion force−displacement ($F_z-\Delta r_z$) curve obtained by differentiating the fitting curve in (a).

Table 2. Force Constants Estimated for the Adhesive Interface in the Tensile Process and Peel Processes 1 and 2

process	tensile	peel 1	peel 2
k (N/m)	86.29	16.55	64.08

displacement width, holding the epoxy molecule and the silica surface together.

Similar to eq 5 for parameter D, the following equation for the force constant seems to hold in approximation.

$$k(\text{tensile}) \approx k_1(\text{peel}) + k_2(\text{peel}) \quad (7)$$

This relationship is similar to that of the spring constants of springs in parallel. For springs in parallel, the overall spring constant can be obtained from the sum of each spring constant. In the same way, it is suggested that when the interaction of the tensile process is considered as one spring, its spring constant can be decomposed into the spring constants of two peeling processes.

Energy and Adhesive Force Decomposition Analysis. In the previous sections, we calculated the adhesion energies

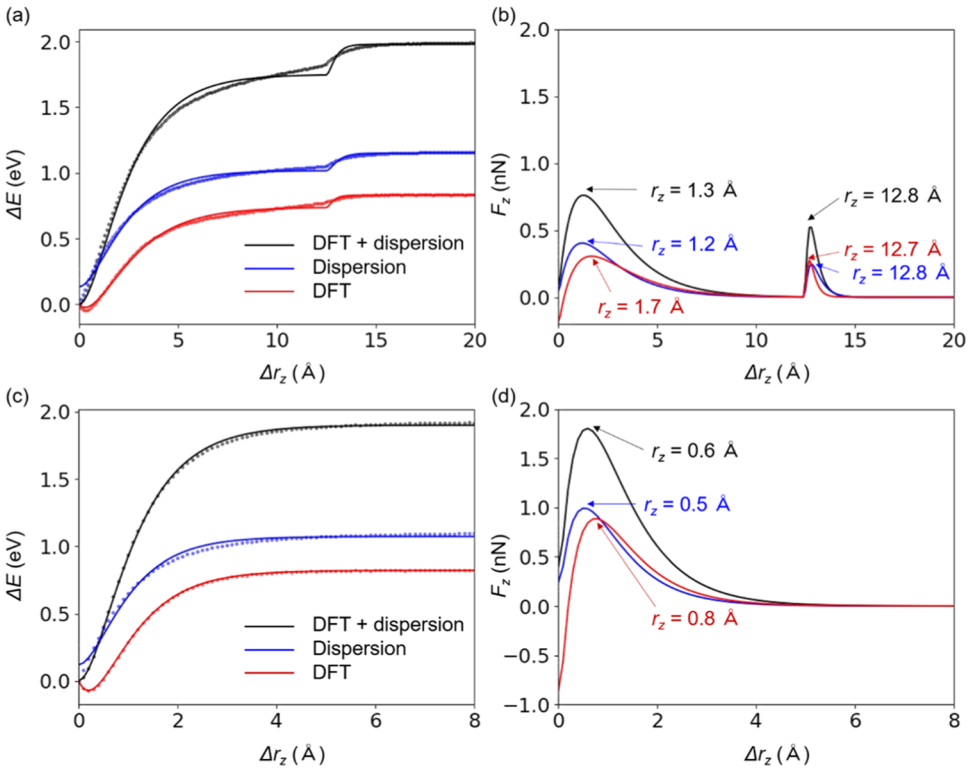

Figure 7. (a) Energy−displacement plot for the peel process (Figure 5a) is decomposed into the DFT and dispersion energies. Each point on the dotted lines corresponds to the value obtained from the calculation, while the solid lines correspond to the fitting curves. The black, blue, and red colors denote the total, dispersion, and DFT energies, respectively. (b) Peel adhesion force−displacement curve for each energy. (c) Energy−displacement plot for the tensile process (Figure 6a) is decomposed into the DFT and dispersion energies. Each point in the dotted line corresponds to the value obtained from the calculation, and the solid lines correspond to the fitting curves. The black, blue, and red colors denote the total, dispersion, and DFT energies, respectively. (d) Tensile adhesion force−displacement curve for each energy.

https://doi.org/10.1021/acsomega.2c01544
ACS Omega 2022, 7, 17393−17400

and forces for the peel and tensile processes for the epoxy/silica interface and confirmed that the peel adhesion force is smaller than the tensile adhesion force. In this section, we perform decomposition analysis of these energies and adhesion forces to explore the origin of the adhesion forces in both processes. In this study, we used the D2 method by Grimme for the dispersion correction. As shown in the following equation, the total energy can be divided into the contributions from the DFT and dispersion correction terms.

$$E_{\mathrm{DFT+disp}} = E_{\mathrm{DFT}} + E_{\mathrm{disp}} \tag{8}$$

By differentiating each term in this equation with respect to the displacement, the adhesion force−displacement curve can be decomposed into two force curves—one derived from the PBE functional (F_{DFT}) and the other from the dispersion force (F_{disp}), which are expressed as

$$F_{\mathrm{DFT+disp}} = F_{\mathrm{DFT}} + F_{\mathrm{disp}} \tag{9}$$

Using this relationship, we performed the decomposition analysis of the energy and force curves for both processes.

In Figure 7a, the energy curve for the peel process in Figure 5a is decomposed into the contributions of the DFT and dispersion correction energies. Each point on the dotted lines is the value obtained from the calculation, while the solid black, blue, and red lines are obtained by fitting: black corresponds to the total energy, blue corresponds to the dispersion energy, and red corresponds to the DFT energy. The blue and red lines were obtained by fitting with the following equation, which is a modification of eq 3.

$$E = D_1(1 - \exp(-a_1(\Delta r_z - \alpha)))^2 + H(\Delta r_z - \Delta r_p)\cdot D_2(1 - \exp(-a_2(\Delta r_z - \Delta r_p)))^2 + \beta \tag{10}$$

The above-mentioned equation differs from eq 3 in that the terms α and β have been added. These two parameters were introduced to account for the different positions of the minima on the energy curves. The parameters for the fitting functions of dispersion and DFT are summarized in Table 3. All of the

Table 3. Fitting Parameters and Coefficients of Determination R^2 for the Energy Curves Shown in Figure 7a,c

Peel							
energy	D_1 (eV)	a_1 (Å^{-1})	D_2 (eV)	a_2 (Å^{-1})	α (Å)	β (eV)	R^2
disp.	0.88	0.57	0.13	2.36	0.0	0.13	0.992
DFT	0.76	0.50	0.09	3.89	0.3	−0.02	0.997
Tensile							
energy	D (eV)	a (Å^{-1})	α (Å)	β (eV)	R^2		
disp.	0.95	1.31	0.0	0.12	0.990		
DFT	0.89	1.24	0.20	−0.07	1.000		

coefficients of determination R^2 for them are above 0.99, in good agreement with the original data points. Numerical differentiation for the fitting curves yielded the peel adhesion force−displacement curves shown in Figure 7b.

In the same way, energy decomposition analysis was performed for the energy curve of the tensile process shown in Figure 6a. The following equation, which is a modification of eq 1, was used for fitting.

$$E = D(1 - \exp(-a(\Delta r_z - \alpha)))^2 + \beta \tag{11}$$

The fitted parameters are summarized in Table 3. The tensile adhesion force−displacement curves were obtained using these fitting parameters (Figure 7d).

From Figure 7b,d, it was found that both dispersion and DFT forces contribute to the adhesion force in both processes, and the peak positions for each force are slightly different. The peak positions for these forces and their adhesion forces for each process are summarized in Table 4. In peel process 1, the

Table 4. Maximum Dispersion and DFT Forces Shown in Figure 7b,d and Their Peak Positions

Peel				
energy	F_1 (nN)	Δr_1 (Å)	F_2 (nN)	Δr_1 (Å)
disp.	0.40	1.2	0.25	12.8
DFT	0.31	1.7	0.28	12.7
Tensile				
energy	F (nN)		Δr (Å)	
disp.	0.99		0.5	
DFT	0.89		0.8	

peak of the DFT force is located at a larger displacement than that of the dispersion force, and this tendency was also observed in the tensile process. As for the adhesive strength, the dispersion force portion is 10−30% larger than the DFT one in both peel 1 and tensile processes. For peel process 2, the values of the dispersion and DFT forces and their peak positions are almost the same. Comparing the adhesive force of peel process 1 with that of the tensile process, the dispersion force in peel is 40% of that in tensile, and the DFT force in peel is 35% of that in tensile.

The peak positions of the dispersion and DFT force curves are different between peel process 1 and the tensile process; the shape of the total force curve is determined by the balance of these forces. This suggests that the dispersion correction is inevitable in the calculation of the adhesive force in the peel and tensile processes.

CONCLUSIONS

For the theoretical investigation of how the adhesive force between the adhesive and adherend changes with fracture direction, the peel and tensile adhesion strengths between a fragment model for DGEBA epoxy resin and the hydroxylated silica surface have been estimated using DFT calculations. Two inflection points were found in the energy curve for the peel process. They are due to the process of the adhesive molecule standing up while rotating with its edge as the rotating shaft and the subsequent dissociation of the vertically oriented adhesive molecule from the surface. The energy curve was fitted well using the function of the sum of two Morse potentials. The energy curve was differentiated to convert it into the force curve. The adhesion force−displacement curve for the peel process has two peaks corresponding to the two inflection points. The adhesion strength was estimated from the peak heights. The estimated peel adhesion strengths are 0.76 and 0.52 nN, both lower than the tensile adhesion strength of 1.80 nN. This result is qualitatively consistent with the trend that the adhesive interface with epoxy resin is vulnerable to fracture in the peeling direction.

https://doi.org/10.1021/acsomega.2c01544
ACS Omega 2022, 7, 17393−17400

To further understand the features of the peel process, force decomposition analysis, which divides the adhesive force into DFT and dispersion forces, was applied to the peel process, and the results were compared with those for the tensile process. As a common feature in both processes, the contribution of the dispersion force to the adhesion force is slightly larger than that of the DFT force. In addition, the force peak due to DFT is located at a larger displacement than that due to dispersion. Both DFT and dispersion forces in the peel process are smaller than those in the tensile process, each being about 40% of the tensile.

■ ASSOCIATED CONTENT

Supporting Information

The Supporting Information is available free of charge at https://pubs.acs.org/doi/10.1021/acsomega.2c01544.

Energy and adhesive force curves for the peel process and tensile process and fitting parameters and adhesion forces for each process of the optimized structures (PDF)

■ AUTHOR INFORMATION

Corresponding Author

Kazunari Yoshizawa − *Institute for Materials Chemistry and Engineering and IRCCS, Kyushu University, Nishi-Ku, Fukuoka 819-0395, Japan;* orcid.org/0000-0002-6279-9722; Email: kazunari@ms.ifoc.kyushu-u.ac.jp

Authors

Yosuke Sumiya − *Institute for Materials Chemistry and Engineering and IRCCS, Kyushu University, Nishi-Ku, Fukuoka 819-0395, Japan*

Yuta Tsuji − *Institute for Materials Chemistry and Engineering and IRCCS, Kyushu University, Nishi-Ku, Fukuoka 819-0395, Japan;* Present Address: Faculty of Engineering Sciences, Kyushu University, 6-1, Kasuga-koen, Kasuga, Fukuoka, 816-8580, Japan; orcid.org/0000-0003-4224-4532

Complete contact information is available at: https://pubs.acs.org/10.1021/acsomega.2c01544

Notes

The authors declare no competing financial interest.

■ ACKNOWLEDGMENTS

This work was supported by KAKENHI grants (numbers JP17K14440, JP17H03117, JP20H05671, and JP21K04996) from the Japan Society for the Promotion of Science (JSPS) and the Ministry of Education, Culture, Sports, Science and Technology of Japan (MEXT) through the MEXT projects Integrated Research Consortium on Chemical Sciences, Cooperative Research Program of Network Joint Research Center for Materials and Devices, and Elements Strategy Initiative to Form Core Research Center and by JST-CREST JPMJCR15P5 and JST-Mirai JPMJMI18A2. The computations in this work were primarily performed using computer facilities at the Research Institute for Information Technology, Kyushu University. Y.T. is grateful for a JSPS Grant-in-Aid for Scientific Research on Innovative Areas (Discrete Geometric Analysis for Materials Design, grant number JP20H04643, and Mixed Anion, grant number JP19H04700).

■ REFERENCES

(1) Kinloch, A. J. The science of adhesion. *J. Mater. Sci.* **1980**, *15*, 2141−2166.

(2) Edward, P. *Epoxy adhesive formulations*; McGraw-Hill Professional, 2005.

(3) Fourche, G. An overview of the basic aspects of polymer adhesion. Part II: Application to surface treatments. *Polym. Eng. Sci.* **1995**, *35*, 968−975.

(4) Fourche, G. An overview of the basic aspects of polymer adhesion. Part I: Fundamentals. *Polym. Eng. Sci.* **1995**, *35*, 957−967.

(5) Petrie, E. M. Epoxy Adhesives. In *Epoxy Adhesive Formulations*, McGraw-Hill Education: New York, 2005; Chapter 1, pp 1−26.

(6) *Advanced Fibre-Reinforced Polymer (FRP) Composites for Structural Applications*, Bai, J., Ed.; Woodhead Publ.: Oxford, 2013.

(7) Chatterjee, S.; Nafezarefi, F.; Tai, N. H.; Schlagenhauf, L.; Nüesch, F. A.; Chu, B. T. T. Size and synergy effects of nanofiller hybrids including graphene nano-platelets and carbon nanotubes in mechanical properties of epoxy composites. *Carbon* **2012**, *50*, 5380−5386.

(8) Ohsako, F.; Yoshizawa, K. Molecular theory of adhesion of metal/epoxy resin interface. *Kobunshi Ronbunshu* **2011**, *68*, 72−80.

(9) Semoto, T.; Tsuji, Y.; Yoshizawa, K. Molecular understanding of the adhesive force between a metal oxide surface and an epoxy resin. *J. Phys. Chem. C* **2011**, *115*, 11701−11708.

(10) Semoto, T.; Tsuji, Y.; Tanaka, H.; Yoshizawa, K. Role of edge oxygen atoms on the adhesive interaction between carbon fiber and epoxy resin. *J. Phys. Chem. C* **2013**, *117*, 24830−24835.

(11) Yoshizawa, K.; Semoto, T.; Hitaoka, S.; Higuchi, C.; Shiota, Y.; Tanaka, H. Synergy of electrostatic and van der Waals interactions in the adhesion of epoxy resin with carbon-fiber and glass surfaces. *Bull. Chem. Soc. Jpn.* **2017**, *90*, 500−505.

(12) Henry, D. J.; Yiapanis, G.; Evans, E.; Yarovsky, I. Adhesion between graphite and modified polyester surfaces: a theoretical study. *J. Phys. Chem. B* **2005**, *109*, 17224−17231.

(13) Köppen, S.; Bronkalla, O.; Langel, W. Adsorption configurations and energies of amino acids on anatase and rutile surfaces. *J. Phys. Chem. C* **2008**, *112*, 13600−13606.

(14) Köppen, S.; Langel, W. Simulation of adhesion forces and energies of peptides on titanium dioxide surfaces. *Langmuir* **2010**, *26*, 15248−15256.

(15) Mian, S. A.; Saha, L. C.; Jang, J.; Wang, L.; Gao, X.; Nagase, S. Density functional theory study of catechol adhesion on silica surfaces. *J. Phys. Chem. C* **2010**, *114*, 20793−20800.

(16) Bahlakeh, G.; Ghaffari, M.; Saeb, M. R.; Ramezanzadeh, B.; De Proft, F.; Terryn, H. A close-up of the effect of iron oxide type on the interfacial interaction between epoxy and carbon steel: combined molecular dynamics simulations and quantum mechanics. *J. Phys. Chem. C* **2016**, *120*, 11014−11026.

(17) Semoto, T.; Tsuji, Y.; Yoshizawa, K. Molecular understanding of the adhesive force between a metal oxide surface and an epoxy resin: effects of surface water. *Bull. Chem. Soc. Jpn.* **2012**, *85*, 672−678.

(18) Mian, S. A.; Yang, L. M.; Saha, L. C.; Ahmed, E.; Ajmal, M.; Ganz, E. A fundamental understanding of catechol and water adsorption on a hydrophilic silica surface: exploring the underwater adhesion mechanism of mussels on an atomic scale. *Langmuir* **2014**, *30*, 6906−6914.

(19) Ogata, S.; Takahashi, Y. Moisture-induced reduction of adhesion strength between surface oxidized Al and epoxy resin: dynamics simulation with electronic structure calculation. *J. Phys. Chem. C* **2016**, *120*, 13630−13637.

(20) Ogata, S.; Uranagase, M. Unveiling the chemical reactions involved in moisture-induced weakening of adhesion between aluminum and epoxy resin. *J. Phys. Chem. C* **2018**, *122*, 17748−17755.

(21) Yoshizawa, K.; Murata, H.; Tanaka, H. Density-functional tight-binding study on the effects of interfacial water in the adhesion force between epoxy resin and alumina surface. *Langmuir* **2018**, *34*, 14428−14438.

(22) Higuchi, C.; Tanaka, H.; Yoshizawa, K. Molecular understanding of the adhesive interactions between silica surface and epoxy resin: Effects of interfacial water. *J. Comput. Chem.* **2019**, *40*, 164−171.
(23) Nakamura, S.; Tsuji, Y.; Yoshizawa, K. Role of hydrogen-bonding and OH-π interactions in the adhesion of epoxy resin on hydrophilic surfaces. *ACS Omega* **2020**, *5*, 26211−26219.
(24) Higuchi, C.; Yoshizawa, K. Energy Decomposition analysis of the adhesive interaction between an epoxy resin layer and a silica surface. *Langmuir* **2021**, *37*, 8417−8425.
(25) Paul, N. C.; Richards, D. H.; Thompson, D. An aliphatic amine cured rubber modified epoxide adhesive: 1. Preparation and preliminary evaluation using a room temperature cure. *Polymer* **1977**, *18*, 945.
(26) Min, K.; Kim, Y.; Goyal, S.; Lee, S. H.; McKenzie, M.; Park, H.; Savoy, E. S.; Rammohan, A. R.; Mauro, J. C.; Kim, H.; Chae, K.; Lee, H. S.; Shin, J.; Cho, E. Interfacial adhesion behavior of polyimides on silica glass: a molecular dynamics study. *Polymer* **2016**, *98*, 1−10.
(27) Tsuji, Y.; Kitamura, Y.; Someya, M.; Takano, T.; Yaginuma, M.; Nakanishi, K.; Yoshizawa, K. Adhesion of epoxy resin with hexagonal boron nitride and graphite. *ACS Omega* **2019**, *4*, 4491−4504.
(28) Tsurumi, N.; Tsuji, Y.; Masago, N.; Yoshizawa, K. Elucidation of adhesive interaction between the epoxy molding compound and Cu lead frames. *ACS Omega* **2021**, *6*, 34173−34184.
(29) Tsuji, Y.; Baba, T.; Tsurumi, N.; Murata, H.; Masago, N.; Yoshizawa, K. Theoretical study on the adhesion interaction between epoxy resin including curing agent and plated gold surface. *Langmuir* **2021**, *37*, 3982−3995.
(30) Ritos, K.; Dongari, N.; Borg, M. K.; Zhang, Y.; Reese, J. M. Dynamics of Nanoscale Droplets on Moving Surfaces. *Langmuir* **2013**, *29*, 6936−6943.
(31) Davim, J. P.; Reis, P.; Antonio, C. C. A study on milling of glass fiber reinforced plastics manufactured by hand-lay up using statistical analysis (ANOVA). *Compos. Struct.* **2004**, *64*, 493−500.
(32) Sethi, S.; Ray, B. C. Environmental effects on fibre reinforced polymeric composites: Evolving reasons and remarks on interfacial strength and stability. *Adv. Colloid Interface Sci.* **2015**, *217*, 43−67.
(33) Zhang, M.; Jianng, B.; Chen, C.; Drummer, D.; Zhai, Z. The effect of temperature and strain rate on the interfacial behavior of glass fiber reinforced polypropylene composites: a molecular dynamics study. *Polymers* **2019**, *11*, 1766.
(34) Barre, S.; Chotard, T.; Benzeggagh, M. L. Comparative study of strain rate effects on mechanical properties of glass fibre reinforced thermoset matrix composites. *Composites, Part A* **1996**, *27A*, 1169−1181.
(35) Min, K.; Rammohan, A. R.; Lee, H. S.; Shin, J.; Lee, S. H.; Goyal, S.; Park, H.; Mauro, J. C.; Stewart, R.; Botu, V.; Kim, H.; Cho, E. Computational approaches for investigating interfacial adhesion phenomena of polyimide on silica glass. *Sci. Rep.* **2017**, *7*, No. 10475.
(36) *Materials Studio 6.1*; Accelrys, Inc.: San Diego, CA, 2012.
(37) Nakamura, S.; Tsuji, Y.; Yoshizawa, K. Molecular Dynamics Study on the Thermal Aspects of the Effect of Water Molecules at the Adhesive Interface on an Adhesive Structure. *Langmuir* **2021**, *37*, 14724−14732.
(38) Kresse, G.; Hafner, J. Ab initio molecular dynamics for liquid metals. *Phys. Rev. B* **1993**, *47*, 558−561.
(39) Kresse, G.; Hafner, J. Ab initio molecular-dynamics simulation of the liquid-metal-amorphous-semiconductor-transition in germanium. *Phys. Rev. B* **1994**, *49*, 14251−14269.
(40) Kresse, G.; Furthmüller, J. Efficiency of ab-initio total energy calculations for metals and semiconductors using a plane-wave basis set. *Comput. Mater. Sci.* **1996**, *6*, 15−50.
(41) Perdew, J. P.; Burke, K.; Ernzerhof, M. Generalized gradient approximation made simple. *Phys. Rev. Lett.* **1996**, *77*, 3865−3868.
(42) Grimme, S. Semiempirical GGA-type density functional constructed with a long-range dispersion correction. *J. Comput. Chem.* **2006**, *27*, 1787−1799.
(43) Kresse, G.; Joubert, D. From ultrasoft pseudopotentials to the projector augmented-wave method. *Phys. Rev. B: Condens. Matter Mater. Phys.* **1999**, *59*, 1758−1775.
(44) Adolph, B.; Furthmüller, J.; Beckstedt, F. Optical properties of semiconductors using projector-augmented waves. *Phys. Rev. B: Condens. Matter Mater. Phys.* **2001**, *63*, No. 125108.
(45) Leng, Y.; Chen, J.; Zhou, B.; Gräter, F. Rupture mechanism of aromatic systems from graphite probed with molecular dynamics simulations. *Langmuir* **2010**, *26*, 10791−10795.
(46) Lechner, C.; Sax, A. F. Adhesive forces between aromatic molecules and graphene. *J. Phys. Chem. C* **2014**, *118*, 20970−20981.
(47) Lechner, C.; Sax, A. F. Towards atomic-level mechanics: adhesive forces between aromatic molecules and carbon nanotubes. *Appl. Surf. Sci.* **2017**, *420*, 606−617.
(48) Milosevic, M. *Internal reflection and ATR spectroscopy*; Wiley: Hoboken, 2012, *21*.
(49) Csaszar, A. G. Structures Averaged Over Nuclear Motions. In *Equilibrium Molecular Structures: From Spectroscopy to Quantum Chemistry*, Demaison, J.; Boggs, J. E.; Csaszar, A. G., Eds.; CRC Press: Boca Raton, 2011; pp 233−262.

https://doi.org/10.1021/acsomega.2c01544
ACS Omega 2022, 7, 17393−17400